Vision and locomotion shape the interactions between neuron types in mouse visual cortex

Mario Dipoppa, Adam Ranson[1], Michael Krumin, Marius Pachitariu, Matteo Carandini[2], and Kenneth D Harris[2]

University College London, London EC1V 9EL, United Kingdom

[1] Present address: Neurosciences & Mental Health Research Institute, Cardiff University, Cardiff CF24 4HQ

[2] Co-senior author

Locomotion profoundly changes sensory responses in mouse primary visual cortex. These changes are thought to arise from a disinhibitory circuit, whereby interneurons expressing vasoactive intestinal peptide (*Vip*) inhibit those expressing somatostatin (*Sst*), thus disinhibiting pyramidal cells (Pyr). We studied the effect of locomotion on these cell types and on interneurons expressing parvalbumin (*Pvalb*) in layer 2/3 of mouse V1, and found inconsistencies with the disinhibitory model. Locomotion increased *Sst* cell responses to large stimuli and to full field gray screen, without decreasing them in *Vip* cells. Moreover, it increased *Vip* cell responses to small stimuli, without decreasing them in *Sst* cells. Signal and noise correlations between cell types provided further evidence against the disinhibitory model. Our data resolve apparent contradictions in the literature and suggest an alternative to the disinhibitory model, where *Vip* and *Sst* cells inhibit each other in a circuit whose effect depends on stimulus and behavioral state.

Introduction

Neocortical interneurons can be divided into genetically distinguishable types, which are arranged in specific functional circuits (Jiang et al., 2015; Kepecs and Fishell, 2014; Markram et al., 2015; Pfeffer et al., 2013; Tasic et al., 2016; Zeisel et al., 2015). There is great interest in understanding how these circuits map to specific features of cortical operation, and how different interneuron types influence each other and ultimately shape the activity of excitatory neurons.

In recent years, a "disinhibitory model" has been proposed as a canonical feature of many cortical areas. This model rests on converging evidence that somatostatin (*Sst*) interneurons are a principal target of interneuron-selective interneurons, such as those expressing vasoactive intestinal peptide (*Vip*). This arrangement has been observed anatomically in the hippocampus (Acsady et al., 1996a; Acsady et al., 1996b), and functionally in auditory cortex (Pi et al., 2013), medial prefrontal cortex (Pi et al., 2013), and visual cortex (Fu et al., 2014; Karnani et al., 2016a; Pfeffer et al., 2013). *Sst* neurons in turn inhibit most other cortical neuronal classes, including pyramidal (Pyr) cells, and *Vip* and parvalbumin (*Pvalb*) interneurons, but not other *Sst* interneurons (Jiang et al., 2015; Karnani et al., 2016b; Pfeffer et al., 2013).

In sensory cortex, this disinhibitory circuit might underlie the modulation of sensory responses by behavioral states such as whisking, arousal, and locomotion. In barrel cortex, for instance, whisking increases the activity of *Vip* cells while decreasing the activity of *Sst* cells, and increases dendritic activity in Pyr neurons (Gentet et al., 2012; Lee et al., 2012). Furthermore, while the activity of Pyr cells correlates strongly with that of *Pvalb* cells, as predicted by the disinhibitory model it correlates weakly or negatively with the activity of *Sst* cells (Gentet et al., 2010; Gentet et al., 2012). In visual cortex, *Vip* cells are activated

when animals run (Fu et al., 2014; Reimer et al., 2014), so a disinhibitory circuit might also explain why visually-driven activity increases during locomotion (Ayaz et al., 2013; Erisken et al., 2014; Niell and Stryker, 2010).

The disinhibitory circuit thus makes a key prediction: that locomotion should decrease the activity of *Sst* neurons. The data in this regard, however, are contradictory. One study reported that running caused a mild but significant reduction in *Sst* neuron activity, thus supporting the hypothesis (Fu et al., 2014), but another study reported the opposite effect (Polack et al., 2013) and yet another found that *Sst* cells can have both behaviors (Reimer et al., 2014).

Indirect evidence to support this prediction comes from visual cortex, where locomotion decreases the strength of a phenomenon, size tuning, that is thought to depend on *Sst* interneurons. Size tuning is the property of many V1 neurons to respond maximally to stimuli of a finite size, while reducing their firing rates to larger stimuli. The magnitude of this reduction relative to the peak response will be operationally defined as the strength of the size tuning effect. *Sst* interneurons are thought to contribute to this effect because they integrate inputs from wide regions of cortex (Adesnik et al., 2012; Zhang et al., 2014) and because suppressing their activity reduces the amount of size tuning (Adesnik et al., 2012). If locomotion reduced their activity via inhibition from *Vip* cells, it should similarly reduce size tuning. This prediction is correct at least in the deep layers of V1 (Ayaz et al., 2013) and, perhaps because of cortical feedback, also in lateral geniculate nucleus (LGN, Erisken et al., 2014).

To investigate these possibilities, and to understand the roles and relationships of different types of interneurons, we systematically investigated the effect of running on visual cortical responses to stimuli of different size. We used two-photon microscopy to measure the activity of genetically-identified *Sst*, *Vip*, and *Pvalb* interneurons, together with pyramidal cells identified either genetically or using a criterion based on the skewness of their calcium traces. Our results indicate that locomotor modulation of each cell class depends critically on the conditions of visual stimulation. As a result, subtle differences in experimental conditions can explain many of the apparent contradictions between previous studies. Our results, moreover, indicate multiple ways in which the disinhibitory model is inconsistent with the observed effects of locomotion. These observations lead us to propose an extension of this model, in which *Vip* and *Sst* cells inhibit each other in a stimulus-dependent winner-take-all circuit.

Results

We used two-photon imaging to measure the activity of Pyr neurons and of *Sst*, *Vip,* and *Pvalb* interneurons in mouse V1 (Figure 1). Mice were head-fixed and free to run on an air-suspended ball (Niell and Stryker, 2010) while viewing a circular horizontal grating drifting downward for 1 s, in windows whose size ranged between 5° and 60° of visual angle (Figure 1A$_1$). We selected for analysis only cells whose receptive field and orientation tuning matched the stimulus, and corrected for out-of-focus fluorescence using previously described methods (Supplementary Figure 1A; Chen et al., 2013; Peron et al., 2015).

Recording the activity of identified cell classes

To identify neurons belonging to a specific class we used one of two approaches (Figure 1A,B). In the first approach, we expressed calcium indicator exclusively in a chosen cell class, by using a triple-transgenic line that expressed the indicator GCaMP6s specifically in superficial layer Pyr cells (Figure 1B$_1$), or by injecting a *Cre*-dependent virus expressing GCaMP6m into an appropriate transgenic driver line (Supplementary Figure 1B$_2$). In the second approach, we injected an unconditional virus to express GCaMP6m in all neurons (Figure 1A$_2$-A$_4$) in double-transgenic mice, where a specific cell class was also labeled with tdTomato. This second approach allowed us to record the activity of identified interneurons together with a large number of unlabeled neurons. These unlabeled neurons are likely to comprise mostly Pyr cells, in addition to interneurons of all classes except the labeled one.

The interneurons of all three classes fired much more frequently than the pyramidal neurons (Figure 1C, D). Superficial-layer pyramidal cells in mouse visual cortex are known to fire sparsely (Niell and Stryker, 2010). Consistent with this notion, the fluorescence traces of a typical genetically-identified pyramidal cell showed rare isolated calcium events (Figure 1C$_1$). Because

events with strong fluorescence were rare in these traces, the distribution of fluorescence was highly skewed (Figure 1D$_1$). By contrast, the typical calcium fluorescence traces of identified *Pvalb, Vip,* and *Sst* interneurons showed frequent calcium events (Figure 1C$_2$-C$_4$), and the corresponding distributions of fluorescence showed little skewness (Figure 1D$_2$-D$_4$). On the other hand, a large number of concurrently measured unlabeled neurons showed sparse activity (example in Figure 1C$_5$) and high skewness (Figure 1D$_5$), resembling the identified Pyr cells (Figure 1C$_1$, D$_1$).

These marked differences in skewness were robust across the population, and allowed us to identify putative Pyr cells among the unlabeled neurons (Figure 1E). Whereas most Pyr cells had skewness values above 3 (81.2%, n = 5,556, Figure 1E$_1$), only a minority of identified interneurons had skewness values above that value (*Pvalb*: 0.5%, n = 192; *Vip*: 2.4%, n = 633; *Sst*: 14.5%, n = 525, Figure 1E$_2$-E$_4$). Unlabeled cells showed a mixture of these two distributions (Figure 1E$_5$). We thus identified unlabeled cells with skewness > 3 as putative Pyr cells.

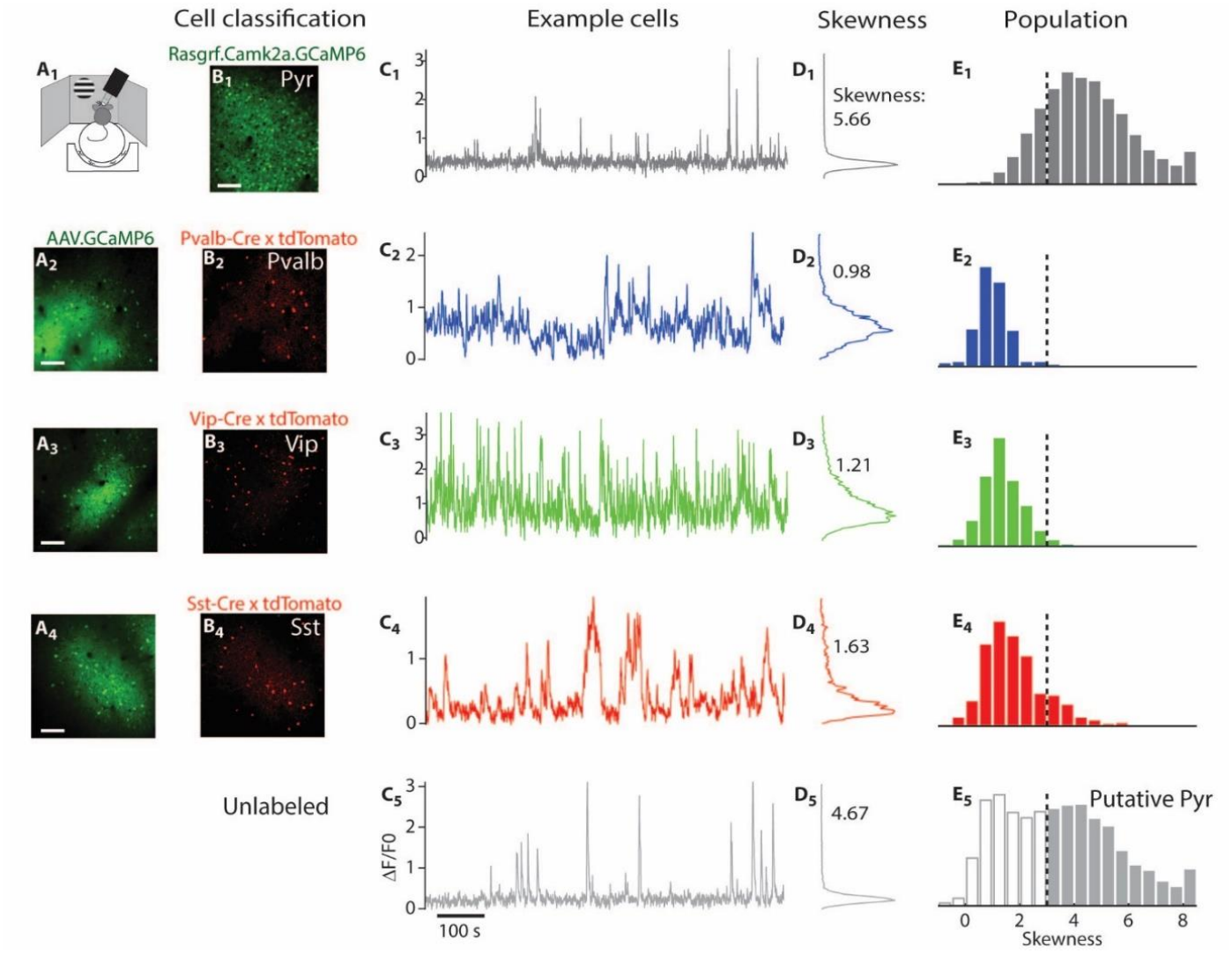

Figure 1. Recordings and classification of Pyr, *Pvalb*, *Vip*, and *Sst* cells in awake mouse V1. (A$_1$) Activity was recorded with two-photon microscopy while visual stimuli were presented. The mouse was free to run on an air-suspended ball. (A$_2$-A$_4$) Green fluorescence from three mice expressing GCaMP6 following virus injection. White bars represent 100 μm. (B$_1$) Green fluorescence from a triple transgenic mouse (Camk2a-tTA; Ai94(TITL-GCaMP6s); Rasgrf2-2A-dCre), which expresses GCaMP6 only in L2/3 Pyr neurons. (B$_2$-B$_4$) Red fluorescence from the recordings in A$_2$-A$_4$, indicating tdTomato expression in *Pvalb* neurons (B$_2$), in *Vip* neurons (B$_3$), and in *Sst* neurons (B$_4$). (C) Calcium traces from five representative neurons of the Pyr, *Pvalb*, *Vip*, *Sst*, and unlabeled types. The unlabeled neuron in C$_5$ was recorded simultaneously with the *Sst* example in C$_4$. The ordinate indicates fluorescence (F) normalized by the baseline fluorescence (F$_0$): ΔF/F$_0$. (D) Histogram of fluorescence values for those five example neurons. The number indicates the skewness of the distribution. (E) Distribution of skewness values over all Pyr, *Pvalb*, *Vip*, *Sst*, and unlabeled neurons.

Effects of locomotion on baseline activity

As a first test of the disinhibitory model, we asked how locomotion affected baseline activity, measured during long periods of gray screen presentation (Figure 2). In *Sst* cells these measurements revealed ways in which previous apparently conflicting reports could be reconciled. In other interneurons, these measurements showed strong effects on baseline activity, an unexpected dependence on cortical depth, and phenomena that run opposite to the predictions of the disinhibitory model.

Consistent with previous results (Niell and Stryker, 2010; Polack et al., 2013; Saleem et al., 2013), locomotion caused diverse but weak effects on the baseline activity of Pyr cells (Figure 2A). The sparse baseline activity of a typical *Pyr* cell correlated weakly with running speed (Figure 2A$_1$). Similar results were seen in the population of identified Pyr cells, where the average correlation of baseline activity and running speed was close to zero ($\rho = 0.01 \pm 0.01$ S.E., n = 5,556 genetically identified Pyr cells), and was significantly positive or negative only in 10% and 13% of the cells (p<.05, shuffle test, Figure 2A$_3$), which nonetheless represented a greater fraction than expected by chance ($p < 10^{-16}$, Fisher's combined probability test). Similar results were seen in the putative Pyr neurons identified by their sparse firing during imaging with unconditional labeling: correlations were small on average ($\rho = -0.04 \pm 0.01$; SE, n = 3,121, Supplementary Figure 2A,B). In agreement with previous results obtained in darkness (Fu et al., 2014), when the monitors were switched off the mean correlation of Pyr activity with speed was again close to zero ($\rho = -0.01 \pm 0.01$, SE, Supplementary Figure 3A$_1$,B$_1$).

The effects of locomotion on the baseline activity of *Pvalb* interneurons were stronger and more varied, and also depended on cortical depth (Figure 2B). For example, in two typical *Pvalb* cells imaged simultaneously (Figure 2B$_1$), activity correlated negatively with running speed in the more superficial cell (darker trace, $\rho = -0.46$, p = 0.03, shuffle test) and positively in the deeper cell (lighter trace, $\rho = 0.48$, $p < 10^{-3}$ shuffle test). These results were typical of the population (n = 192), where the correlations were strong and depended significantly on depth ($p < 10^{-3}$; Figure 2B$_2$). Among *Pvalb* cells in superficial L2/3 (depth <300 µm, n = 129) the overall correlation with speed was negative (-0.16 ± 0.03, SE), and this correlation was significantly negative in 31% of the cells and significantly positive only in 8% of the cells (p<.05; shuffle test). The situation was reversed in deeper L2/3 (n = 63), where *Pvalb* cells showed an overall weak positive correlation with speed ($\rho = 0.09 \pm 0.05, \mathrm{SE}$), with correlations significantly positive in 38% of cells and negative in only 13% of cells (p<.05; shuffle test). When pooling across depth, therefore, a wide variety of effects was seen (Figure 2B$_3$), echoing the wide and bimodal range of correlations observed in darkness (Fu et al., 2014).

Also in agreement with previous observations (Fu et al., 2014), *Vip* interneurons showed a very different behavior: their baseline activity correlated strongly and positively with locomotion (Figure 2C). The typical *Vip* cell increased baseline activity markedly with locomotion (Figure 2C$_1$), and the overall population showed almost exclusively positive correlations with running speed, with a mean correlation of 0.23 ± 0.01 (SE, n = 633). This correlation was significantly positive in 60% of cells and negative in only 2% of the cells (p<.05; shuffle test), with correlation increasing mildly but significantly with cortical depth ($p < 10^{-5}$; Z-test). We found similar results when we repeated these measurements in darkness ($\rho = 0.14 \pm 0.01$, SE, Supplementary Figure 3A$_2$,B$_2$).

Contrary to the predictions of the disinhibitory circuit, however, strong positive correlations with locomotion were also seen in the baseline activity of *Sst* interneurons (Figure 2D). The typical *Sst* cell increased its baseline activity markedly with locomotion (Figure 2D$_1$) and across the population the correlation of baseline activity with running speed was on average positive (0.18 ± 0.01, SE, n = 525), and only marginally dependent on depth (p = 0.046; Z-test, Figure 2D$_2$). The resulting distribution was significantly positive in 49% of cells, and negative in only 7% of cells (p<.05, shuffle test; Figure 2D$_3$). These effects of locomotion on the baseline activity of *Sst* interneurons confirm some previous results (Polack et al., 2013) but they appear to disagree with other measurements (Fu et al., 2014). Indeed, they run opposite to the predictions of the disinhibitory circuit, which would have predicted

negative effect of locomotion on baseline activity of *Sst* cells.

To confirm the validity of these results, we first ensured that they were not due to possible contamination from background fluorescence originating in other cell classes. We repeated the measurements in *Sst-IRES-Cre* mice where the calcium indicator was expressed only in *Sst* cells by injecting a Cre-dependent GCaMP6m virus (Supplementary Figure 1B$_2$); the virus was injected in adult animals, thus excluding the off-target expression that might occur in cells that expressed Cre only transiently during development (Hu et al., 2013). These experiments confirmed our original results: where GCaMP6 was strongly expressed– whether cell bodies or neuropil – the average correlation of baseline activity with running speed was positive (Supplementary Figure 1D$_2$-E$_2$). A pixel-by-pixel analysis further confirmed that these results did not depend on our specific method of ROI detection (Supplementary Figure 1C).

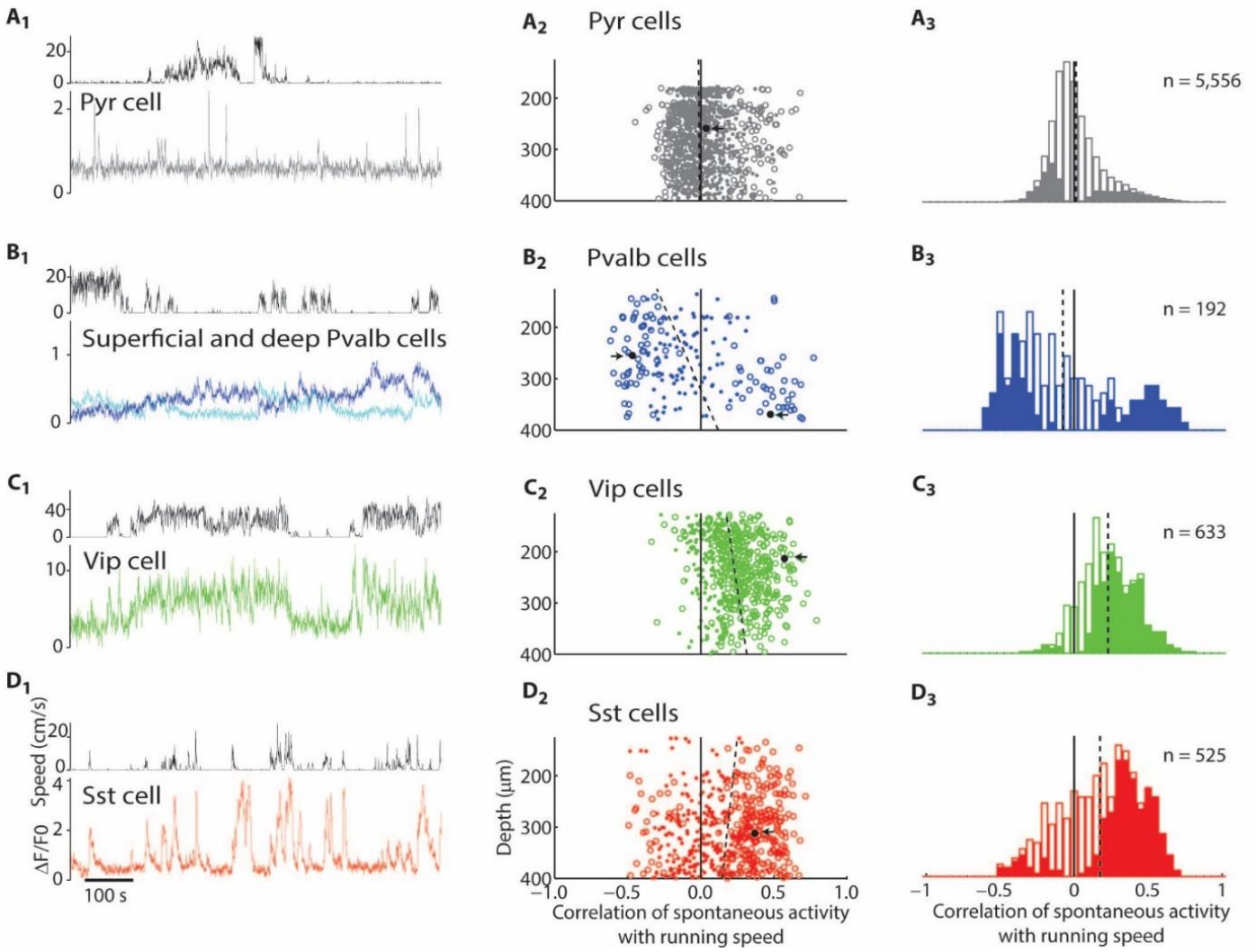

Figure 2. Correlates of running with neural activity in absence of visual stimuli (gray screen). (A$_1$) Fluorescence of representative L2/3 pyramidal neuron (top) and simultaneous running speed trace (bottom). (A$_2$) Correlation coefficient of recorded pyramidal cells with running speed, plotted vs. cell depth. Circles represent cells with significant correlations at p<0.05 (shuffle test); dots represent cells with insignificant correlations. For clearer visualization we plotted only a random subsample of 20% of genetically-identified Pyr cells. Dashed line represents fitted dependence of correlation vs. depth. Arrow indicates example cell shown in A$_1$. (A$_3$) Histogram of correlation coefficients of all pyramidal cells. Solid bars indicate significant correlations at p<0.05 (shuffle test). (B) Similar analysis for *Pvalb* neurons. The two traces in B$_1$ (top) show fluorescence traces of representative *Pvalb* cells of upper and lower L2/3 (blue and cyan). (C) Similar analysis for *Vip* cells. (D) Similar analysis for *Sst* cells.

We next asked if the disagreement on the effects of locomotion on the baseline activity of *Sst* cells could be due to different visual conditions used in different experiments. The experiments of Fu et al. (2014) were performed in darkness, whereas in ours (Figure 2D), and those of Polack et al. (2013), the mouse faced a gray screen. A gray screen can provide effective visual stimulation, particularly to *Sst* cells whose large receptive field (Adesnik et al., 2012) may encompass the edges of the screens, which create high contrast. We thus repeated our measurements of *Sst* baseline activity in darkness, and found that the effects of running were again diverse, but were now overall negative rather than positive ($\rho = -0.12 \pm 0.01$, SE; $p < 10^{-12}$ t-test, Supplementary Figure $3A_3$,B_3,C), just as in the experiments of Fu et al. (2014).

These measurements, therefore, reconcile the apparent divergence of previous results: the effect of running on baseline activity of *Sst* cells is overall positive when mice view a gray screen (Figure 2D and Polack et al., 2013), and mildly negative when mice are in darkness (Supplementary Figure $3A_3$,B_3,C and Fu et al., 2014). The disinhibitory model, however, is consistent only with the observations made in darkness, not the observations made with the gray screen.

Effects of locomotion on responses to gratings of different sizes

The previous analysis highlights the importance of controlling visual stimulation when studying the effects of locomotion. These effects could be radically different depending on whether they were measured in the dark or in the presence of a gray screen. We thus asked how locomotion affects the responses to stimuli of different sizes. To determine the specific effect of locomotion on the visual responses, in this analysis we measured responses to stimuli (drifting gratings) relative to baseline activity measured prior to stimulus onset. We selected only cells that were visually responsive (significant effect of stimulus size, $p < 0.05$, 1-way ANOVA) and whose receptive field was centered within 10° of the center of the visual stimulus. Amongst Pyr neurons with clear orientation tuning (orientation selectivity index > 0.2), we selected only those whose preferred orientation differed by <45° from the stimulus.

The responses of genetically identified L2/3 Pyr cells showed strong selectivity for small stimuli (in agreement with Adesnik et al., 2012), and exhibited only a mild effect of locomotion (Figure 3A). The responses of a typical Pyr neuron were substantially stronger to a 5° stimulus than to a 60° stimulus, regardless of locomotion (Figure $3A_1$). Accordingly, the tuning curves showed clear selectivity for stimulus size, i.e. size tuning for both this cell (Figure $3A_2$) and the overall population of genetically identified Pyr cells (n = 607; Figure $3A_3$). On average, locomotion slightly increased responses to both small stimuli ($p < 10^{-6}$, paired t-test) and large stimuli ($p < 10^{-3}$, paired t-test). However, this effect was highly diverse among cells, with locomotion significantly increasing or decreasing responses in 16% and 6% of Pyr cells respectively ($p<.05$; 2-way ANOVA, main effect of running over 5° and 60° stimuli, Figure $3A_4$). This diversity was accompanied by a diversity in size tuning across cells (Supplementary Figure 4). Many cells (23%) showed a significant interaction of running and stimulus size ($p<.05$; 2-way ANOVA over 5° and 60° stimuli; Figure $3A_4$). In these cells, locomotion changed the relative response to large and small stimuli, as seen previously in deeper layers (Ayaz et al., 2013). Similar results were found in putative pyramidal cells identified by the sparseness of their calcium traces (Supplementary Figure 2C,D).

Pvalb interneurons showed similar selectivity for stimulus size, but a stronger and almost invariably positive effect of locomotion (Figure 3B). A typical *Pvalb* interneuron responded strongly to small stimuli and more weakly to larger stimuli, and its responses markedly increased during locomotion (Figure $3B_1$-B_2). These effects were highly consistent across *Pvalb* interneurons (n = 37, Figure $3B_3$), with locomotion increasing firing rate in practically all cells (Figure $3B_4$). This effect was seen in responses to both large stimuli ($p < 10^{-3}$, paired t-test) and small stimuli ($p < 10^{-4}$, paired t-test), with no significant interaction between stimulus size and locomotion ($p = 0.79$, within subject repeated measures ANOVA over 5° and 60° stimuli).

In *Vip* interneurons, running generally increased responses to small stimuli, but contrary to the predictions of the disinhibitory circuit, it did little to the responses to large stimuli (Figure 3C). A typical *Vip* interneuron responded most strongly to small stimuli

during locomotion (Figure 3C$_1$-C$_2$). Similar results were seen across the population: *Vip* interneurons showed clear size tuning, and running increased their responses both to 5° stimuli ($p < 10^{-10}$, n = 83, paired t-test) and to 60° stimuli ($p < 10^{-4}$, paired t-test, Figure 3C$_3$). However, the effect was stronger for small stimuli, with a significant interaction of size and locomotion ($p < 0.01$, within subject repeated measures ANOVA over 5° and 60° stimuli; Figure 3C$_4$). Similarly to baseline activity, we found that modulation of visual responses by running grew with cortical depth ($p < 10^{-4}$, Z-test; Supplementary Figure 5).

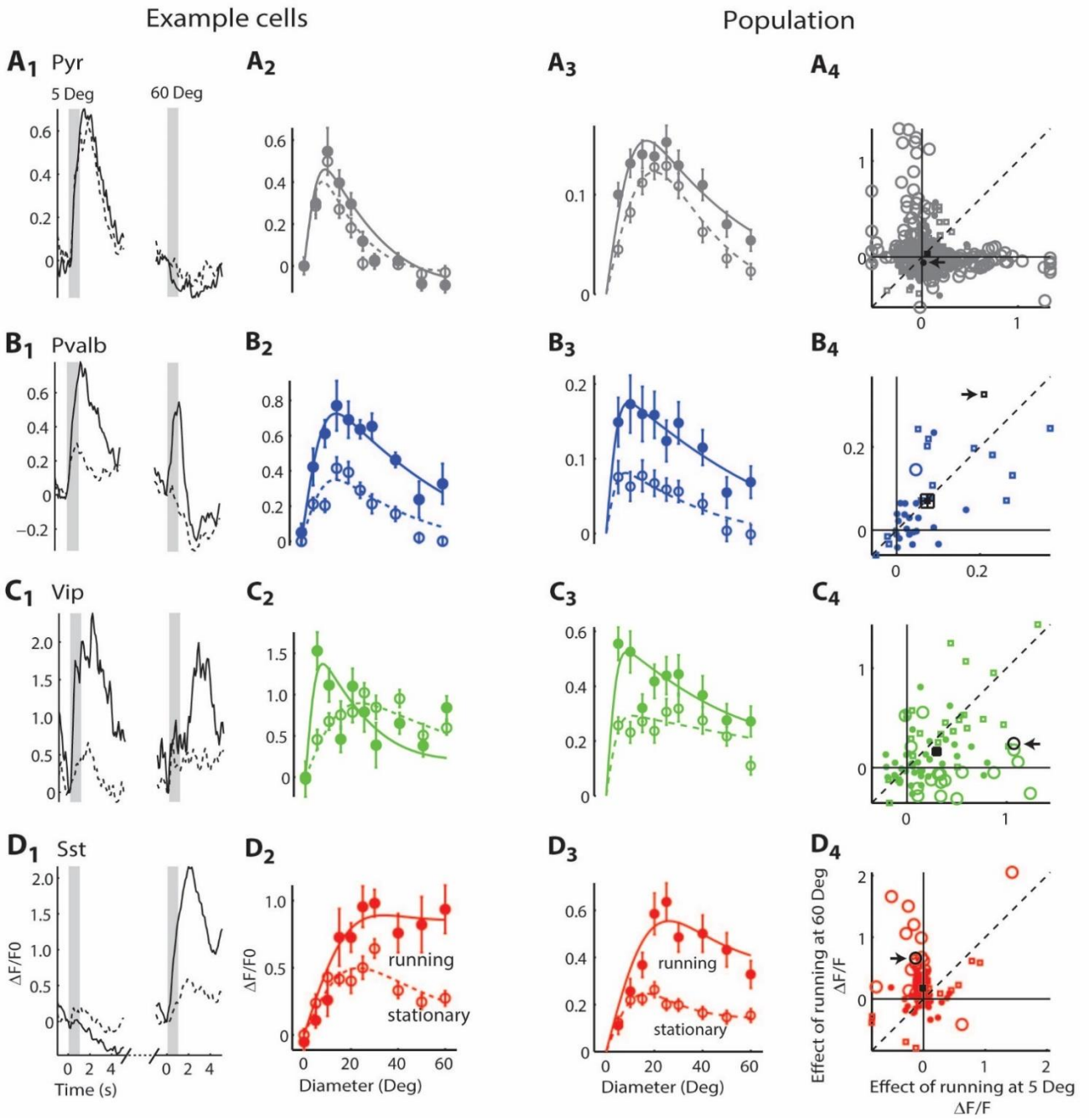

Figure 3. Running increases visual responses for large drifting grating stimuli in *Sst* neurons, for small stimuli in *Vip* neurons, and for all stimulus sizes in *Pvalb* neurons. (A$_1$) Responses of a representative Pyr neuron. Black curves show trial-averaged response in the stationary (dashed line) and running (continuous line) conditions. Panels show responses to stimuli of 5° (left) and 60° (right). Gray shaded regions indicate the 1 s stimulus presentation period. (A$_2$) size tuning curve for this example cell. Solid line: running; dashed line: stationary. (A$_3$) Size tuning curve, averaged over Pyr cells. Solid line: running; dashed line: stationary. (A$_4$) Scatter plot showing change with running of responses to large stimuli (60°; y-axis) and to small stimuli (5°; x-axis). Circles represent cells whose responses have a significant interaction between size and running (multi-way ANOVA over 5° and 60° stimuli only), squares represent cells that did not have a significant interaction but did have a significant effect of running; dots represent cells with no significant effect of locomotion. Arrow marks example cell shown in A$_{1-2}$, square marks mean response. (B-D), similar analysis for *Pvalb*, *Vip*, and *Sst* neurons.

Sst interneurons responded preferentially to large stimuli, and contrary to the predictions of the disinhibitory circuit these responses increased with running (Figure 3D). Consistent with the data of Adesnik et al. (2012), a typical *Sst* interneuron gave weak responses to small stimuli, and strong responses to larger stimuli, which became even larger if the animal was running (Figure 3D$_1$, D$_2$). Similar results were seen across the population (n = 110, Figure 3D$_3$), with overall activity peaking for stimuli of ~20° during stationary conditions, and ~30° during running. Some *Sst* cells showed clear size tuning (Supplementary Figure 4C,D). This observation differs from those of Adesnik et al. (2012) and may reflect high sensitivity of these cells to stimulus centering (Supplementary Figure 6). In the centered *Sst* cells, nevertheless, there was a significant interaction between stimulus size and locomotion ($p < 10^{-4}$, within subject repeated measures ANOVA over 5° and 60° stimuli). While running did not significantly affect the responses to small stimuli (p = 0.64, paired t-test, Figure 3D$_4$), opposite to the predictions of the disinhibitory circuit it strongly increased the responses to large stimuli ($p < 10^{-4}$, paired t-test).

For large stimuli, therefore, our results contradict the disinhibitory model, which predicts that locomotion should increase firing in *Vip* cells and decrease it in *Sst* cells. Instead, we saw something closer to the opposite behavior: when large stimuli are present, locomotion does little to *Vip* cells, and markedly increases the activity of *Sst* cells.

Correlations of interneuron activity with putative pyramidal activity

To further test the disinhibitory model, we examined the patterns of correlation between different interneuron types and Pyr cells (Figure 4). To measure correlation, we relied on our ability to record simultaneously the activity of identified interneurons and of sparse-firing putative Pyr neurons (Figure 1). This analysis revealed dramatic differences between interneuron classes.

Consistent with the view that *Pvalb* interneurons track the activity of Pyr cells (Cruikshank et al., 2007; Isaacson and Scanziani, 2011; Okun and Lampl, 2008; Ozeki et al., 2009; Renart et al., 2010), we found strong positive correlations between the *Pvalb* and *Pyr* populations, regardless of locomotion (Figure 4A). In each experiment, we summed the activity of the *Pvalb* interneurons and compared it to the summed activity of the simultaneously recorded putative Pyr cells. Only cells whose receptive field lay within 10° from the stimulus center were considered. In a typical experiment the spontaneous correlations (ρ_0) measured in the presence of a gray screen were strongly positive, whether the mouse was stationary ($\rho_0 = 0.64$, Figure 4A$_1$) or running ($\rho_0 = 0.31$, Figure 4A$_2$). Similar results were seen across all experiments ($\rho_0 = 0.54 \pm 0.10$, SE, during stationarity and 0.35 ± 0.14 during running). Examining population signal correlations – i.e. the relationship of the mean summed responses of the *Pvalb* and Pyr cells across stimuli – also showed a strong, positive correlation in both stationary ($\rho_s = 0.66$ for the example in Figure 4A$_3$, 0.81 ± 0.08 across all experiments) and running conditions ($\rho_s = 0.90$ for the example in Figure 4A$_4$, 0.88 ± 0.02 SE across all experiments). Similar results were also found for population noise correlations (i.e. the relationship between trial-to-trial variability in summed activity of the *Pvalb* and Pyr populations; Supplementary Figure 7). The high positive linear correlation of the *Pvalb* and Pyr populations is consistent with the prevalent view that *Pvalb* cells track the summed activity of the Pyr population during spontaneous activity, stimulus responses, and trial-to-trial fluctuations (Isaacson and Scanziani, 2011).

Vip cells showed a markedly different behavior. Their correlations with Pyr populations differed from those of *Pvalb* cells in two respects. First, while spontaneous and noise correlations tended to be positive ($\rho_0 = 0.27 \pm 0.33$, SE, during stationarity and 0.61 ± 0.16 during running; $\rho_n = 0.10 \pm 0.09$, SE, during stationarity and 0.23 ± 0.12 during running), they were weaker than those of *Pvalb* cells, at least during stationarity (Fig. 4D$_{1,2}$ and Supplementary Figure 7). Second, the relationship between the population mean responses of *Vip* and Pyr cells showed clear evidence of nonlinearity during running conditions (Figure 4B$_4$). This nonlinearity reflects the observation that *Vip* and Pyr populations show qualitatively different size tuning during running, with *Vip* cells peaking at smaller stimulus sizes (compare Figs. 3C$_3$ and 3A$_3$). It further suggests that, unlike for *Pvalb* cells, the sensory tuning

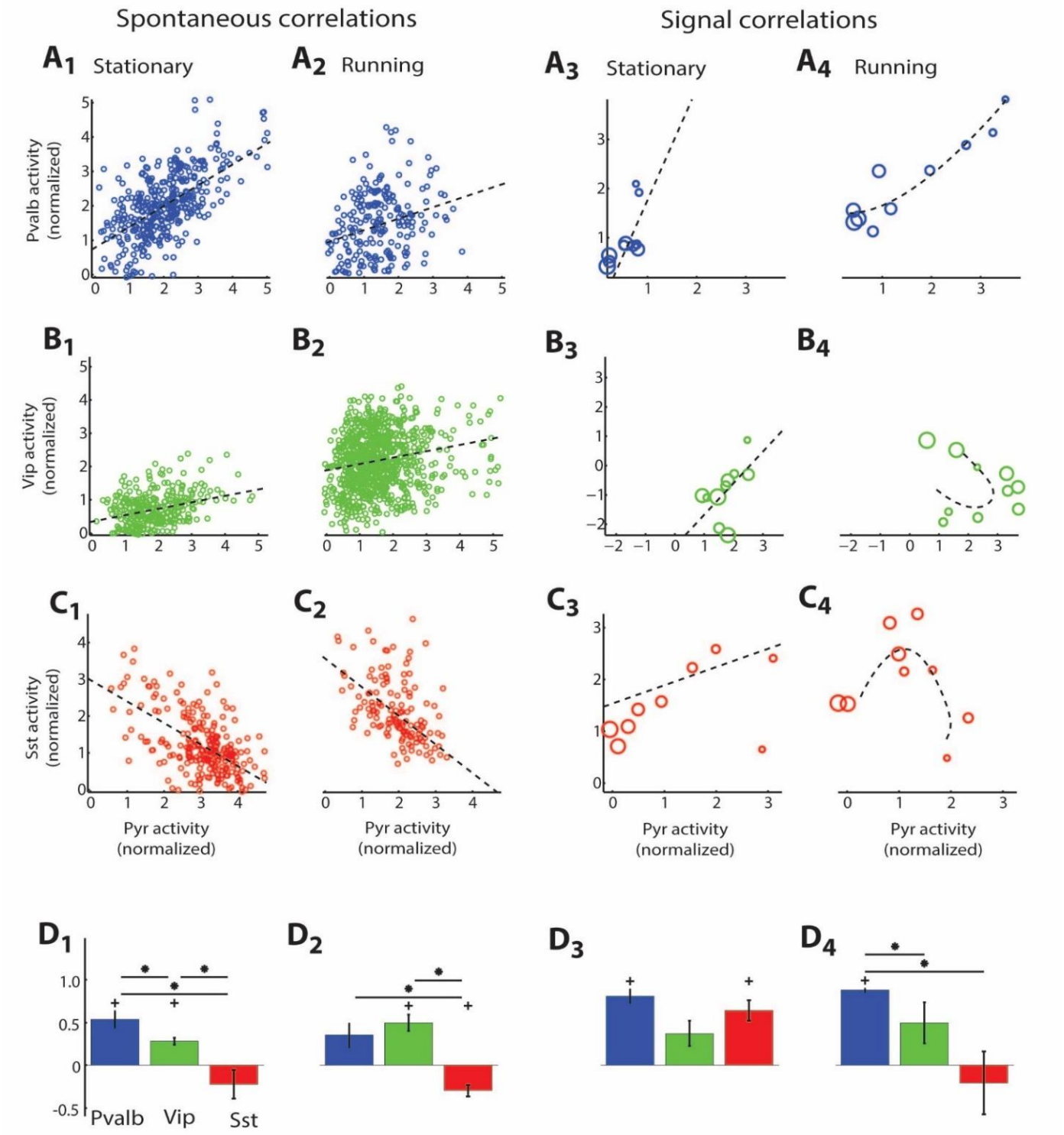

Figure 4. Correlations of interneuron classes and simultaneously recorded putative pyramidal cells. (A_1) Summed activity of *Pvalb* population vs. Pyr population in the gray screen condition during stationary periods. (A_2) Same as A_1 during running. (A_3) Average stimulus response of *Pvalb* population vs. average response of Pyr population in a typical experiment during stationary periods. Dashed line indicates linear regression estimate of signal correlation (A_4) Same as A_1 but during running. (B) Same as A, for *Vip* interneurons. Note the nonlinear signal correlation during running (B_4), which was fit using the tuning curves of the *Vip* and Pyr populations (c.f. Figs. $3A_3$, $3C_3$). (C) Same as A, for *Sst* interneurons. (D_1) Summary plots of spontaneous correlations during stationary periods. Crosses mark significant differences to zero ($p < 0.05$, t-test), asterisks correspond to populations with significantly different correlations ($p < 0.05$, unpaired t-test). (D_2) Same as D_1 during running.

of *Vip* cells during running cannot be explained by a simple tracking of excitatory activity.

Sst interneurons showed yet a different sort of behavior. Consistent with previous results in somatosensory cortex (Gentet et al., 2012), the correlation of the *Sst* and Pyr populations was weak or negative, both in stationary conditions ($\rho_0 = -0.64$ for the example in Figure 4C$_1$, -0.22 ± 0.17 SE across all experiments), and during running (ρ_0 = -0.53 for the example in Figure 4C$_2$, -0.30 ± 0.07 SE across all experiments). Noise correlations were also weak or negative (Supplementary Figure 7; $\rho_n = 0.05 \pm 0.18$ SE, stationary, $\rho_n = -0.18 \pm 0.07$ SE, running). Signal correlations showed a complex interaction of running and stimulus size. During stationary conditions, signal correlations tended to be positive ($\rho_s = 0.91$ in the example, Figure 4C$_3$). But during running the relationship between the population mean responses of *Sst* and Pyr cells was again nonlinear (Figure 4C$_4$). The weak or negative spontaneous and noise correlations indicate that the activity of the *Sst* population again cannot be determined primarily by tracking of local excitatory activity, and is instead consistent with suppression of Pyr activity by *Sst* cells. However, the running-dependent and nonlinear relationship between the mean response of these two populations indicates that suppression of Pyr activity by *Sst* cells is unlikely to fully account for their size tuning under all conditions.

Overall, thus, these results paint a more complex picture than would be expected from the disinhibitory model. The model predicts that Pyr activity should increase with *Vip* activity and decrease with *Sst* activity. This prediction is consistent with correlations measured during spontaneous activity, but is not consistent with the covariation of stimulus responses seen in the presence of large stimuli, which shows the opposite pattern of activity. Visual stimulation, therefore, creates situations where the disinhibitory circuit is incorrect.

Discussion

Our results indicate that one cannot simply ask whether locomotion increases or decreases the activity of a particular cell class: the effects of locomotion in mouse V1 interact with the precise sensory conditions present, in a manner that varies between cell classes and even with cortical depth. We found that locomotion increased sensory responses in all cell classes, with the increase being most prominent for large stimuli in *Sst* cells, for small stimuli in *Vip* cells, not strongly dependent on stimulus size for *Pvalb* cells, and with diverse size-dependence amongst individual pyramidal neurons. The effects of locomotion on baseline neural activity (as assessed by gray screen viewing) were more complex: locomotion generally increased activity in *Sst* neurons; strongly increased activity in *Vip* neurons, and had diverse effects on *Pvalb* and Pyr cells, generally decreasing activity of *Pvalb* cells in superficial L2/3 and increasing activity in deeper cells.

Our results indicate that apparent discrepancies in the previous literature may in fact reflect subtly different paradigms used in different experiments. For example, a previous study reported very weak size tuning in *Sst* cells during running (Adesnik et al., 2012). Although we observed robust size tuning in stationary animals, this was greatly reduced during locomotion, when it was indeed absent unless we restricted analysis to the most centered cells in our database. In two other studies on the spontaneous activity of *Sst* cells, one reported an increase with locomotion (Polack et al., 2013), while another reported a decrease (Fu et al., 2014). When we replicated the conditions of both studies (gray screen for the first study, complete darkness for the second), we replicated both of their results in the same neurons. This result reconciles the apparent contradiction between these previous studies.

Our results also reinforce the importance of correcting for out-of-focus fluorescence in 2-photon calcium imaging. Indeed, without correcting for this confound, one would observe an artifactual negative correlation of fluorescence with running speed, specifically in image regions where GCaMP was not expressed strongly (Supplementary Figure 1).

We had set out to test a specific, simple “disinhibitory” hypothesis: that during locomotion, increased activity of *Vip* cells would inhibit *Sst* cells, and thus increase the activity of pyramidal cells (Fu et al., 2014). While many of our results were consistent with the hypothesis, others could not be explained by this simple model alone. We confirmed that locomotion increased responses in *Vip* interneurons. But while the

disinhibitory model predicts that increased *Vip* activity should suppress *Sst* firing, we found that *Sst* firing instead increased during locomotion, as long as visual inputs were present (even a blank gray screen). This increase in *Sst* firing with running must therefore reflect a mechanism other than the simple disinhibitory circuit; while this mechanism is currently unknown, one possibility could be the action of muscarinic acetylcholine receptors. Previous work has implicated acetylcholine in the depolarization of V1 *Vip* cells during running, through the action of nicotinic receptors (Fu et al., 2014); although *Sst* cells do not express nicotinic receptors, they do express muscarinic acetylcholine receptors, which can have a strong depolarizing effect (Chen et al., 2015; Fanselow et al., 2008; Kawaguchi, 1997).

Intriguingly, the effects of locomotion on *Vip* and *Sst* cells depended on the stimulus in a complementary manner. When large grating stimuli were present, running strongly boosted *Sst* cell activity, but had little effect on *Vip* cells. Conversely, when small stimuli were present, *Vip* cells showed the greater increase in activity. These results suggest that locomotion might set up a competitive interaction between these two mutually inhibitory interneuron types (Karnani et al., 2016b; Pfeffer et al., 2013). *Vip* cells have a narrow dendritic and axonal structure that suggests a highly localized role in cortical processing (Jiang et al., 2015; Karnani et al., 2016a), while *Sst* cells receive input from a retinotopically wide area of the local cortical region (Adesnik et al., 2012; Zhang et al., 2014). The presentation of small visual stimuli, combined with excitation caused by locomotion (Figure 5A) may thus synergistically excite *Vip* cells, causing them to suppress *Sst* neurons. Conversely presentation of large visual stimuli during locomotion (Figure 5B) may synergistically drive *Sst* cells, causing them to suppress *Vip* cell activity. This mutual suppression model may explain a large number of our current observations, including the complementary size tuning of *Vip* and *Sst* cells during running; the nonlinear relationship of their average responses to stimuli of different sizes with those of the Pyr population; and the signs of their respective spontaneous and noise correlations with summed local Pyr activity.

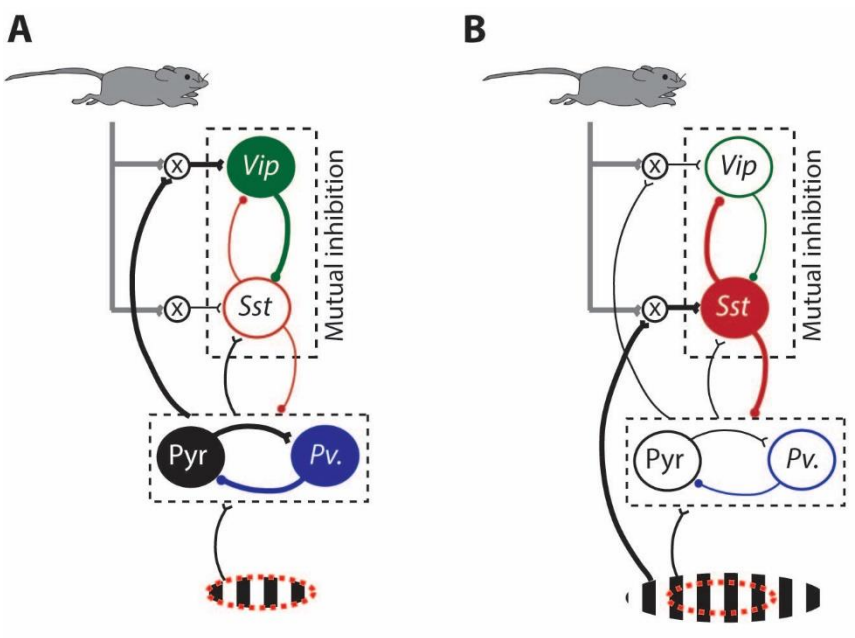

Figure 5. Hypothesized mechanism for the interaction between running and size tuning in L2/3 of mouse V1. While *Pvalb* interneurons closely track the summed firing of the Pyr population, the *Vip* and *Sst* populations are both excited by running, leading to a stimulus-dependent competition between them. (A) When the stimulus is small, the disinhibitory mechanism holds: the *Vip* population receives stronger input, suppressing the *Sst* population, and relieving Pyr and *Pvalb* cells from inhibition. (B) When the stimulus is large, the disinhibitory mechanism is reversed: *Sst* cells receive greater net input, suppressing *Vip* cells and also inhibiting Pyr and *Pvalb* cells.

In contrast to the complex relationship of *Vip* and *Sst* neurons to summed Pyr activity, the activity of *Pvalb* interneurons was in all cases tightly locked to the local excitatory population. These data are therefore consistent with a model in which *Pvalb* cells receive strong excitatory input, serving primarily to stabilize the activity of the local circuit via tracking summed excitatory firing (Figure 5; Cruikshank et al., 2007; Ozeki et al., 2009; Renart et al., 2010).

What computational benefit might the interaction of locomotion, stimulus size, and cell type serve in visual

cortex? One can consider two hypotheses for why visual cortical activity should be modulated by running. In the first hypothesis, boosting of activity in visual cortex in running animals serves as a form of modality-specific attention: because vision is particularly important during spatial navigation, locomotion increases V1 activity while suppressing the activity of competing sensory systems. While this is supported by the fact that locomotion appears to decrease activity in other cortical regions (Schneider et al., 2014; Zhou et al., 2014), it cannot explain why the effects of locomotion on V1 pyramidal cells are so diverse, boosting some while decreasing others, as well as boosting responses only to certain sensory stimuli (Keller et al., 2012; Saleem et al., 2013). The second hypothesis holds that locomotor modulation of V1 is not simply a matter of gain control, but a detailed integration of visual and locomotor input, that critically depends on diverse neuronal integration of these two input streams. Indeed, work in virtual reality environments has suggested that, rather than simply making visual responses larger or smaller, locomotor modulation may underlie more complex computations, such as integrating the animal's own movement with that of the world (Keller et al., 2012; Saleem et al., 2013). Diverse interaction of sensory stimuli and locomotion in different interneuron classes might form a key mechanism behind this integration.

Methods

Mice

Experiments in which an interneuron class was labelled with tdTomato and recorded together with other cells were conducted in double-transgenic mice obtained by crossing Gt(ROSA)26Sor<tm14(CAG-tdTomato)Hze> reporters (Madisen et al., 2010) with appropriate drivers: *Pvalb*<tm1(cre)Arbr> (Hippenmeyer et al., 2005) (2 males, 2 females), *Vip*<tm1(cre)Zjh> (Taniguchi et al., 2011) (1 male, 2 females), and *Sst*<tm2.1(cre)Zjh> (Taniguchi et al., 2011) (2 males). These mice are referred to as *Pvalb* x tdTom, *Vip* x tdTom and *Sst* x tdTom, respectively. Experiments in which indicator was expressed uniquely in one interneuron class were conducted in single transgenic mice: *Vip*<tm1(cre)Zjh> (n=1), and *Sst*<tm2.1(cre)Zjh> (n=3), referred to as *Vip-Cre* and *Sst*-Cre respectively. Experiments in which pyramidal cells were labelled exclusively were conducted in *CamK2a*-tTA; Ai94(TITL-GCaMP6s); *Rasgrf2*-2A-dCre triple transgenic mice (n=3) (Madisen et al., 2015).

Ten mice were housed under reversed light-dark (12h and 12h) conditions after surgery and for the duration of the experiments, while six mice were housed in normal light condition. Mice were used for experiments at adult postnatal ages (P54-110). All experimental procedures were conducted according to the UK Animals Scientific Procedures Act (1986). Experiments were performed at University College London under personal and project licenses released by the Home Office following appropriate ethics review.

Animal preparation and virus injection

In experiments where an interneuron class was recorded together with other cells, mice were injected with an unconditional GCaMP6m virus, AAV1.Syn.GCaMP6m.WPRE.SV40 (referred to as non-flex.GCaMP6m). In experiments where an interneuron class was labelled by unique expression, mice were injected with AAV1.Syn.Flex.GCaMP6m.WPRE.SV40 (flex.GCaMP6m) and AAV2/1.CAG.FLEX.tdTomato.WPRE.bGH (flex.tdTomato). In both cases, viruses were loaded in a beveled sharp micropipette mounted on a Nanoject II device (Drumond) attached to a micromanipulator. All injections were performed in adult mice (P35–P76), and in the same procedure they were head-implanted in a stereotaxic frame while under anesthesia (decreasing level of isofluorane from 4.5% to 0.75% during the surgery). One-three boli of 100-200 nl virus (dilution: 2.23 10^{12} GC/ml for non-flex.GCaMP6m; 2.71 10^{12} for flex.GCaMP6m) were stereotaxically injected unilaterally into monocular V1 (Wagor et al., 1980) 2.1-3.3 mm laterally from Bregma and at a depth of L2/3 (200-400 µm). All viruses (AAVs) were acquired from University of Pennsylvania Viral Vector Core.

In Vivo Calcium Imaging

Experiments were performed 16-34 days after virus injection (P54-110). We used a B-scope (ThorLabs, Ely UK), with an acquisition frame rate of about 30Hz which (corresponding for each plane to a rate of 4-6 Hz) is then interpolated to a frequency of 10 Hz common

to all planes. Recordings occurred in the area where expression was strongest. In most recordings (n = 14) this location was in the monocular zone (MZ, horizontal visual field preference > 30°)(Wagor et al., 1980). Other recordings (n = 2) were performed in the callosal binocular zone (CBZ, n= 1, 0-15°)(Wang and Burkhalter, 2007) and others (n = 4) in the acallosal binocular zone (ABZ, 15-30°).

Visual stimuli and experimental protocol

Horizontal gratings were projected in a visual location adjusted to match the center of GCaMP expression, on one of two screens that together spanned -45 to +135 deg of the horizontal visual field and ±42.5 deg of the vertical visual field (Figure 1A$_1$). During gray screen presentation, the screens were set to a steady gray level equal to the background of all the stimuli presented for visual responses protocols. Stimuli had a temporal frequency of 2 Hz and spatial frequency of 0.15 cycles per degree.

Calcium data processing

Raw calcium movies were realigned to account for brain motion using a registration algorithm (Guizar-Sicairos et al., 2008). Regions of interest (ROIs) were semi-automatically identified using custom algorithms, with post-hoc manual curation to distinguish somata from dendritic processes based on their morphology. Cells expressing tdTomato were identified semi-automatically using an algorithm based on their average fluorescence in the red channel. Pyramidal neurons were identified by their high skweness (Fig. 1), computed during long recordings of visual stimulation (size tuning) and gray stimulus presentation (when present).

Pixel maps of calcium data

To confirm the correlation of running speed and fluorescence independent of ROI detection, we computed correlation maps (Supplementary Figure 1C), showing for each pixel, the Pearson correlation between the activity of the pixel and the running speed (c.f. Freeman et al. (2014)). Prior to correlation, the activity of each pixel was smoothed by convolving with a spatial Gaussian with standard deviation equal to 1.5 pixels, and a temporal Hamming window of 1 s width.

The correlation of baseline fluorescence with running speed varied across the field of view. In regions where GCaMP was expressed strongly, baseline fluorescence correlated positively with running speed, likely indicating an increase in axonal and dendritic activity in locomoting animals. However, in areas where GCaMP fluorescence was weak, the correlation of the background with running speed was negative, likely indicating increased hemodynamic filtering of the light due to stronger blood flow during running (Huo et al., 2015). To ensure this did not affect our results, we removed background fluorescence from the detected fluorescence of recorded neurons (see below).

Background fluorescence correction

With two-photon GCaMP imaging, an important concern is that out-of-focus fluorescence can contaminate the signal ascribed to particular neurons; this is of particular concern in situations where the surrounding GCaMP-labelled neuropil may itself show modulation by stimuli or behaviors such as locomotion. In order to correct out-of-focus contamination, we adopted the method of (Peron et al., 2015). A “neuropil mask” was defined as the region up to 35 μm microns from the ROI border, excluding pixels corresponding to other detected cells. The fluorescence in this mask was subtracted from the raw cell trace with a correction factor equal to 1 (Supplementary Figure 1A). We verified that this correction factor was appropriate for our data by examining the lower envelope of the relationship between neuropil and somatic fluorescence, which had a slope close to 1 for all cells (example in Supplementary Figure 1A$_2$).

Analysis of neural activity

The average fluorescence was defined by $\Delta F/F_0 = (F-F_0)/F_0$, where F is the average raw calcium signal during the first second of the stimulus presentation, and F_0 is the global minimum of the fluorescence trace after smoothing with a 10-point average filter (time between two time points is 0.1 s). The correlation of neural activity with running speed during gray screen presentation was assessed by the Pearson correlation coefficient between the calcium signal and the running speed trace, on an interpolated timebase of 10 Hz, smoothed (5 points) and decimated (1 Hz). To ascertain the significance of this correlation we used a shuffling

method, in which the speed trace was randomly circularly shifted relative to the fluorescence trace 1,000 times – this was necessary because serial correlation in the timeseries of fluorescence and speed rendered successive samples statistically dependent.

The size of a cell's response to a stimulus was defined by the difference of $\Delta F/F_0$ between the first 1 s of the stimulus period, and the 1 s of baseline activity prior to stimulus presentation. A neuron was determined to have a significant response to the stimulus using a paired t-test of the hypothesis that fluorescence during rest vs. locomotion come from distributions with equal means.

To measure each cell's retinotopic location, in the majority of datasets (n = 16) receptive fields were obtained from responses to sparse, uncorrelated noise. The screen was divided into squares of 5 by 5 degrees, and each square was independently turned on and off randomly at a 5Hz overall rate. At any time, 5% of all squares were on. For each neuron, each cell's response to each square was obtained using stimulus-triggered averaging. The receptive fields were smoothed in space and their peak was identified as the preferred spatial position. In a subset of early experiments (n = 4), receptive fields were assessed with flickering vertical or horizontal bars appearing in different locations; we verified in a further n = 4 datasets that the two measures of a cell's receptive field were consistent.

Author contributions

M.D. performed the experiments and analyzed the data; M.D., A.R. and M.P. performed surgeries; A.R. and M.K. built the two-photon set-up; M.D, M.K. and M.P. implemented the retinotopic mapping software; K.D.H. and M.P. implemented the ROI detection algorithms; M.D., A.R., M.C. and K.D.H. designed the experiments; M.D., M.C. and K.D.H. wrote the paper with inputs from all authors.

Acknowledgments

We thank Charu Reddy for transgenic mouse breeding and maintenance, performing surgeries and technical support, Chris Burgess for building the data acquisition software set-up, Luigi Federico Rossi for assistance during surgeries, Miles Wells for assistance in mice habituation, Sylvia Schroeder for implementing the retinotopic mapping software. For the use of GCaMP6f we acknowledge Vivek Jayaraman, Rex A. Kerr, Douglas S. Kim, Loren L. Looger, Karel Svoboda from the GENIE Project, Janelia Farm Research Campus, Howard Hughes Medical Institute. This work was supported by the Wellcome Trust. MD was supported by a Marie Curie Intra-European Fellowship for Career Development, KDH by EPSRC, MC holds the GlaxoSmithKline / Fight for Sight Chair in Visual Neuroscience.

References

Acsady, L., Arabadzisz, D., and Freund, T.F. (1996a). Correlated morphological and neurochemical features identify different subsets of vasoactive intestinal polypeptide-immunoreactive interneurons in rat hippocampus. Neuroscience 73, 299-315.

Acsady, L., Gorcs, T.J., and Freund, T.F. (1996b). Different populations of vasoactive intestinal polypeptide-immunoreactive interneurons are specialized to control pyramidal cells or interneurons in the hippocampus. Neuroscience 73, 317-334.

Adesnik, H., Bruns, W., Taniguchi, H., Huang, Z.J., and Scanziani, M. (2012). A neural circuit for spatial summation in visual cortex. Nature 490, 226-231.

Ayaz, A., Saleem, A.B., Scholvinck, M.L., and Carandini, M. (2013). Locomotion controls spatial integration in mouse visual cortex. Current biology : CB 23, 890-894.

Chen, N., Sugihara, H., and Sur, M. (2015). An acetylcholine-activated microcircuit drives temporal dynamics of cortical activity. Nature neuroscience 18, 892-902.

Chen, T.W., Wardill, T.J., Sun, Y., Pulver, S.R., Renninger, S.L., Baohan, A., Schreiter, E.R., Kerr, R.A., Orger, M.B., Jayaraman, V., *et al.* (2013). Ultrasensitive fluorescent proteins for imaging neuronal activity. Nature 499, 295-300.

Cruikshank, S.J., Lewis, T.J., and Connors, B.W. (2007). Synaptic basis for intense thalamocortical activation of feedforward inhibitory cells in neocortex. Nature neuroscience 10, 462-468.

Erisken, S., Vaiceliunaite, A., Jurjut, O., Fiorini, M., Katzner, S., and Busse, L. (2014). Effects of locomotion extend throughout the mouse early visual system. Current biology : CB 24, 2899-2907.

Fanselow, E.E., Richardson, K.A., and Connors, B.W. (2008). Selective, state-dependent activation of somatostatin-expressing inhibitory interneurons in mouse neocortex. Journal of neurophysiology 100, 2640-2652.

Freeman, J., Vladimirov, N., Kawashima, T., Mu, Y., Sofroniew, N.J., Bennett, D.V., Rosen, J., Yang, C.T., Looger, L.L., and Ahrens, M.B. (2014). Mapping brain activity at scale with cluster computing. Nature methods 11, 941-950.

Fu, Y., Tucciarone, J.M., Espinosa, J.S., Sheng, N., Darcy, D.P., Nicoll, R.A., Huang, Z.J., and Stryker, M.P. (2014). A cortical circuit for gain control by behavioral state. Cell 156, 1139-1152.

Gentet, L.J., Avermann, M., Matyas, F., Staiger, J.F., and Petersen, C.C. (2010). Membrane potential dynamics of GABAergic neurons in the barrel cortex of behaving mice. Neuron 65, 422-435.

Gentet, L.J., Kremer, Y., Taniguchi, H., Huang, Z.J., Staiger, J.F., and Petersen, C.C. (2012). Unique functional properties of somatostatin-expressing GABAergic neurons in mouse barrel cortex. Nature neuroscience 15, 607-612.

Guizar-Sicairos, M., Thurman, S.T., and Fienup, J.R. (2008). Efficient subpixel image registration algorithms. Opt Lett 33, 156-158.

Hippenmeyer, S., Vrieseling, E., Sigrist, M., Portmann, T., Laengle, C., Ladle, D.R., and Arber, S. (2005). A developmental switch in the response of DRG neurons to ETS transcription factor signaling. PLoS biology 3, e159.

Hu, H., Cavendish, J.Z., and Agmon, A. (2013). Not all that glitters is gold: off-target recombination in the somatostatin-IRES-Cre mouse line labels a subset of fast-spiking interneurons. Frontiers in neural circuits 7, 195.

Huo, B.X., Gao, Y.R., and Drew, P.J. (2015). Quantitative separation of arterial and venous cerebral blood volume increases during voluntary locomotion. Neuroimage 105, 369-379.

Isaacson, J.S., and Scanziani, M. (2011). How inhibition shapes cortical activity. Neuron 72, 231-243.

Jiang, X., Shen, S., Cadwell, C.R., Berens, P., Sinz, F., Ecker, A.S., Patel, S., and Tolias, A.S. (2015). Principles of connectivity among morphologically defined cell types in adult neocortex. Science 350, aac9462.

Karnani, M.M., Jackson, J., Ayzenshtat, I., Hamzehei Sichani, A., Manoocheri, K., Kim, S., and Yuste, R. (2016a). Opening Holes in the Blanket of Inhibition: Localized Lateral Disinhibition by VIP Interneurons. The Journal of neuroscience : the official journal of the Society for Neuroscience 36, 3471-3480.

Karnani, M.M., Jackson, J., Ayzenshtat, I., Tucciarone, J., Manoocheri, K., Snider, W.G., and Yuste, R. (2016b). Cooperative Subnetworks of Molecularly Similar Interneurons in Mouse Neocortex. Neuron 90, 86-100.

Kawaguchi, Y. (1997). Selective cholinergic modulation of cortical GABAergic cell subtypes. Journal of neurophysiology 78, 1743-1747.

Keller, G.B., Bonhoeffer, T., and Hubener, M. (2012). Sensorimotor mismatch signals in primary visual cortex of the behaving mouse. Neuron 74, 809-815.

Kepecs, A., and Fishell, G. (2014). Interneuron cell types are fit to function. Nature 505, 318-326.

Lee, S.H., Kwan, A.C., Zhang, S., Phoumthipphavong, V., Flannery, J.G., Masmanidis, S.C., Taniguchi, H., Huang, Z.J., Zhang, F., Boyden, E.S., *et al.* (2012). Activation of specific interneurons improves V1 feature selectivity and visual perception. Nature 488, 379-383.

Madisen, L., Garner, A.R., Shimaoka, D., Chuong, A.S., Klapoetke, N.C., Li, L., van der Bourg, A., Niino, Y., Egolf, L., Monetti, C., *et al.* (2015). Transgenic mice for intersectional targeting of neural sensors and effectors with high specificity and performance. Neuron 85, 942-958.

Madisen, L., Zwingman, T.A., Sunkin, S.M., Oh, S.W., Zariwala, H.A., Gu, H., Ng, L.L., Palmiter, R.D., Hawrylycz, M.J., Jones, A.R., *et al.* (2010). A robust and high-throughput Cre reporting and characterization system for the whole mouse brain. Nature neuroscience 13, 133-140.

Markram, H., Muller, E., Ramaswamy, S., Reimann, M.W., Abdellah, M., Sanchez, C.A., Ailamaki, A., Alonso-Nanclares, L., Antille, N., Arsever, S., *et al.* (2015). Reconstruction and Simulation of Neocortical Microcircuitry. Cell 163, 456-492.

Niell, C.M., and Stryker, M.P. (2010). Modulation of visual responses by behavioral state in mouse visual cortex. Neuron 65, 472-479.

Okun, M., and Lampl, I. (2008). Instantaneous correlation of excitation and inhibition during ongoing and sensory-evoked activities. Nature neuroscience 11, 535-537.

Ozeki, H., Finn, I.M., Schaffer, E.S., Miller, K.D., and Ferster, D. (2009). Inhibitory stabilization of the cortical network underlies visual surround suppression. Neuron 62, 578-592.

Peron, S.P., Freeman, J., Iyer, V., Guo, C., and Svoboda, K. (2015). A Cellular Resolution Map of Barrel Cortex Activity during Tactile Behavior. Neuron 86, 783-799.

Pfeffer, C.K., Xue, M., He, M., Huang, Z.J., and Scanziani, M. (2013). Inhibition of inhibition in visual cortex: the logic of connections between molecularly distinct interneurons. Nature neuroscience 16, 1068-1076.

Pi, H.J., Hangya, B., Kvitsiani, D., Sanders, J.I., Huang, Z.J., and Kepecs, A. (2013). Cortical interneurons that specialize in disinhibitory control. Nature 503, 521-524.

Polack, P.O., Friedman, J., and Golshani, P. (2013). Cellular mechanisms of brain state-dependent gain modulation in visual cortex. Nature neuroscience 16, 1331-1339.

Reimer, J., Froudarakis, E., Cadwell, C.R., Yatsenko, D., Denfield, G.H., and Tolias, A.S. (2014). Pupil Fluctuations Track Fast Switching of Cortical States during Quiet Wakefulness. Neuron 84, 355-362.

Renart, A., de la Rocha, J., Bartho, P., Hollender, L., Parga, N., Reyes, A., and Harris, K.D. (2010). The asynchronous state in cortical circuits. Science 327, 587-590.

Saleem, A.B., Ayaz, A., Jeffery, K.J., Harris, K.D., and Carandini, M. (2013). Integration of visual motion and locomotion in mouse visual cortex. Nature neuroscience 16, 1864-1869.

Schneider, D.M., Nelson, A., and Mooney, R. (2014). A synaptic and circuit basis for corollary discharge in the auditory cortex. Nature 513, 189-194.

Taniguchi, H., He, M., Wu, P., Kim, S., Paik, R., Sugino, K., Kvitsiani, D., Fu, Y., Lu, J., Lin, Y., *et al.* (2011). A resource of Cre driver lines for genetic targeting of GABAergic neurons in cerebral cortex. Neuron 71, 995-1013.

Tasic, B., Menon, V., Nguyen, T.N., Kim, T.K., Jarsky, T., Yao, Z., Levi, B., Gray, L.T., Sorensen, S.A., Dolbeare, T., *et al.* (2016). Adult mouse cortical cell taxonomy revealed by single cell transcriptomics. Nature neuroscience 19, 335-346.

Wagor, E., Mangini, N.J., and Pearlman, A.L. (1980). Retinotopic organization of striate and extrastriate visual cortex in the mouse. The Journal of comparative neurology 193, 187-202.

Wang, Q., and Burkhalter, A. (2007). Area map of mouse visual cortex. The Journal of comparative neurology 502, 339-357.

Zeisel, A., Munoz-Manchado, A.B., Codeluppi, S., Lonnerberg, P., La Manno, G., Jureus, A., Marques, S., Munguba, H., He, L., Betsholtz, C., *et al.* (2015). Brain structure. Cell types in the mouse cortex and hippocampus revealed by single-cell RNA-seq. Science 347, 1138-1142.

Zhang, S., Xu, M., Kamigaki, T., Hoang Do, J.P., Chang, W.C., Jenvay, S., Miyamichi, K., Luo, L., and Dan, Y. (2014). Selective attention. Long-range and local circuits for top-down modulation of visual cortex processing. Science 345, 660-665.

Zhou, M., Liang, F., Xiong, X.R., Li, L., Li, H., Xiao, Z., Tao, H.W., and Zhang, L.I. (2014). Scaling down of balanced excitation and inhibition by active behavioral states in auditory cortex. Nature neuroscience 17, 841-850.

Supplemental Figures

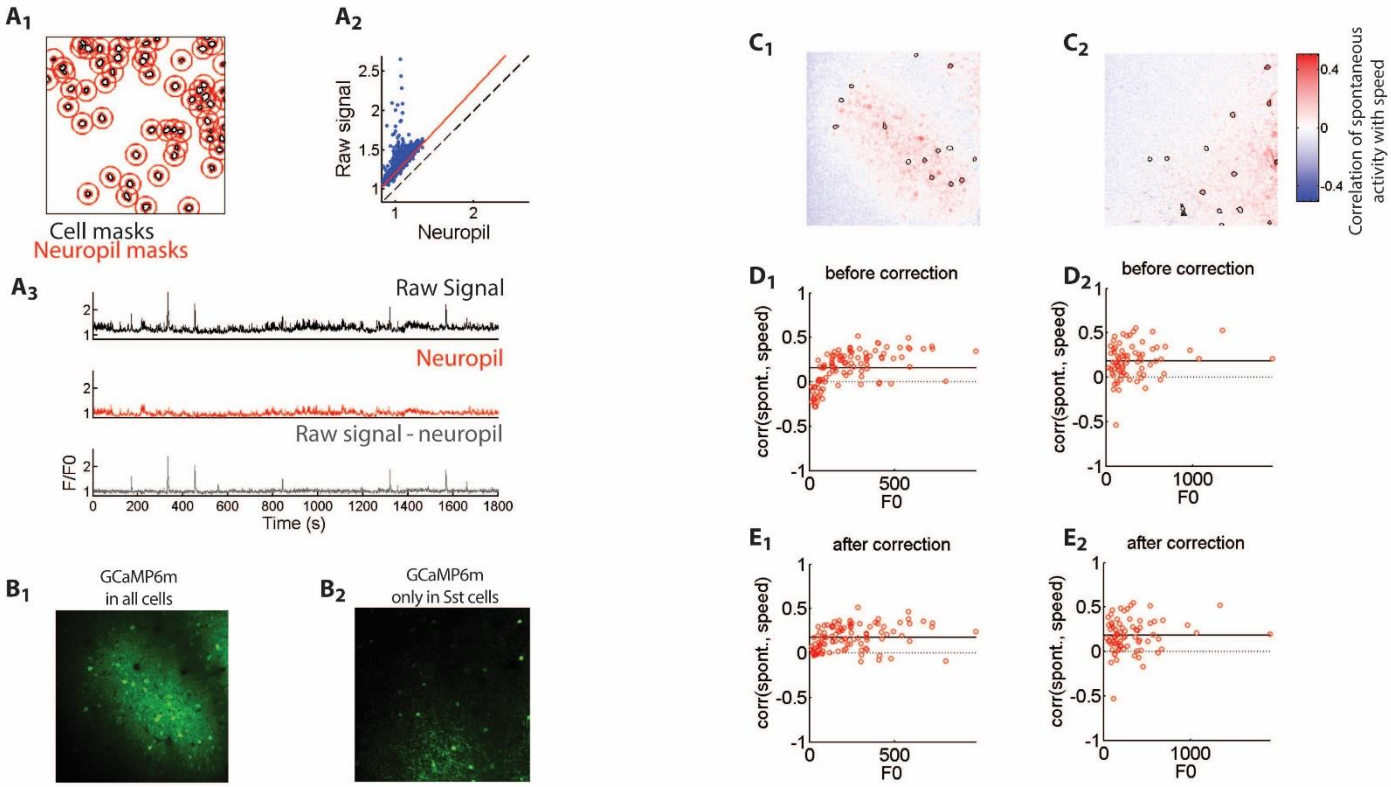

Supplementary Figure 1, related to Figures 1 and 2. Background fluorescence correction. (A_1) For every cell, a "neuropil mask" was defined, extending 35 µm circularly from the cell's center, and excluding any pixels belonging to detected neurons. (A_2) Scatter plot of the raw signal vs. neuropil trace (1 point every 1s). Red line: fit of the lower 5% percentile of the scatter plot, showing a slope of 1.06. As all cells showed slopes close to 1, we subtracted a multiple of 1 of the neuropil signal from each cell's fluorescence trace. (A_3) Example raw signal trace (top), neuropil trace (center), and corrected signal trace (bottom). (B) Map showing mean GCaMP fluorescence level: (B_1) GCaMP expressed in all neurons (same field of view as in Figure $1A_4$); (B_2): GCaMP is expressed only in Sst neurons. (C) Maps showing correlation of running speed with fluorescence for each pixel, for the same fields of view shown in B_1 and B_2. Black contours represent outlines of detected Sst cells, detected by tdTomato expression (c.f. B_1 and Fig. $1A_4$, $1B_4$) or by GCaMP expression (c.f. B_2). Note that while positive correlations are seen in regions where GCaMP is strongly expressed, negative correlations are seen in regions of low GCaMP expression, presumably reflecting hemodynamic filtering. (D, E) Correlation of fluorescence with running speed, as a function of baseline fluorescence level F0, before (D) and after (E) neuropil subtraction for these two fields of view. Continuous black lines represent the average correlation in each plot. Note that prior to neuropil subtraction in the experiment with unconditional expression, a negative correlation is observed in cells of with very weak GCaMP expression, similarly to the surrounding neuropil.

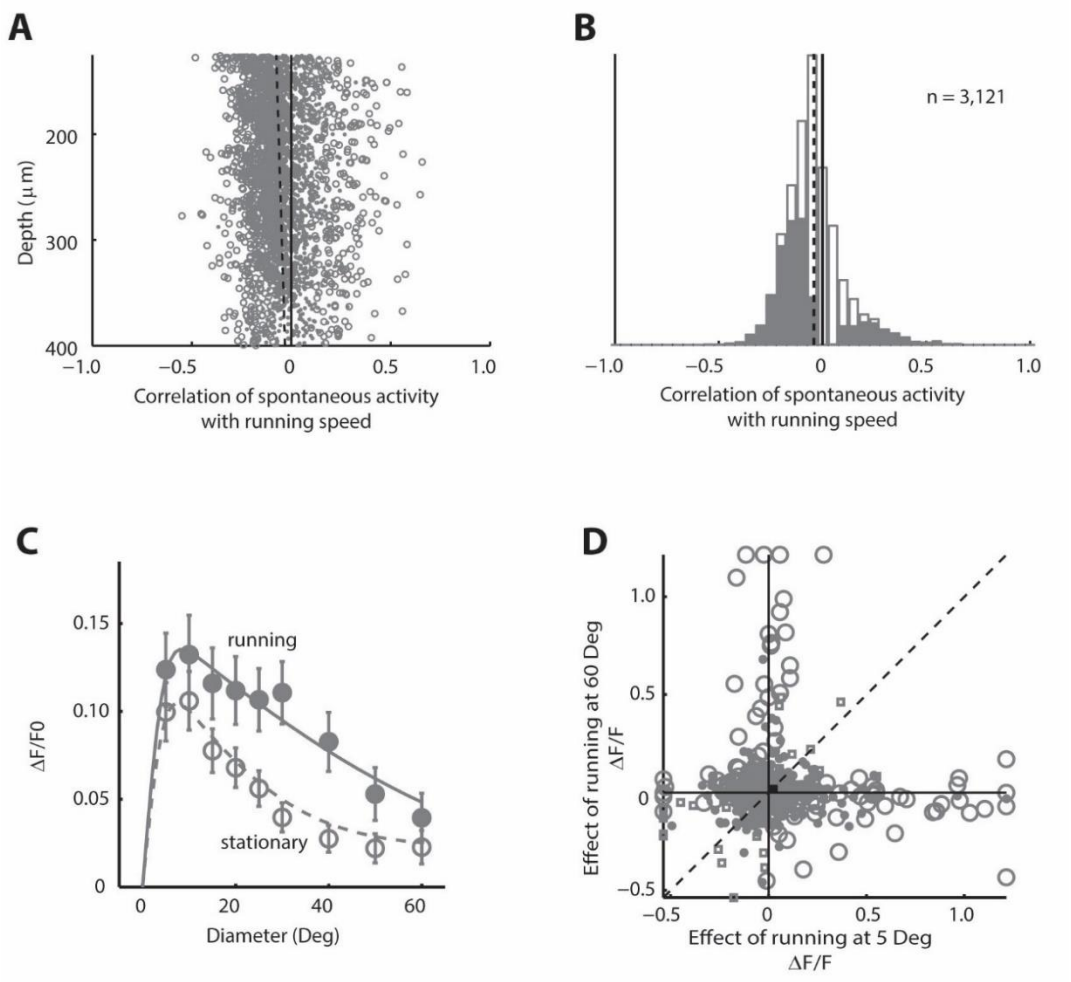

Supplementary Figure 2, related to Figure 2. Size tuning and running modulation in putative Pyr cells identified by sparse firing. (A) Correlation of neural fluorescence with running speed as a function of cell depth. Circles indicate cells with significant correlations at $p<0.05$ (shuffle test), dots indicate cells of insignificant correlation. Dashed line corresponds to a linear fit of correlation vs. depth. (B) Marginal histogram of correlation values for cells. Filled portions of bars indicate cells that are significantly modulated by speed. Correlations were significantly positive or negative in 9% and 35% of cells ($p<.05$, shuffle test). (C) Mean size tuning curve averaged over all cells. (D) Scatter plots showing modulation by running of responses to large stimuli (y-axis) and small stimuli (x-axis). Circles correspond to cells whose responses have a significant interaction between size and running ($p<0.05$, two-way ANOVA over 5° and 60° stimuli); squares correspond to cells that did not have a significant interaction but did have a significant effect of running; dots correspond to cells with no significant effect of running.

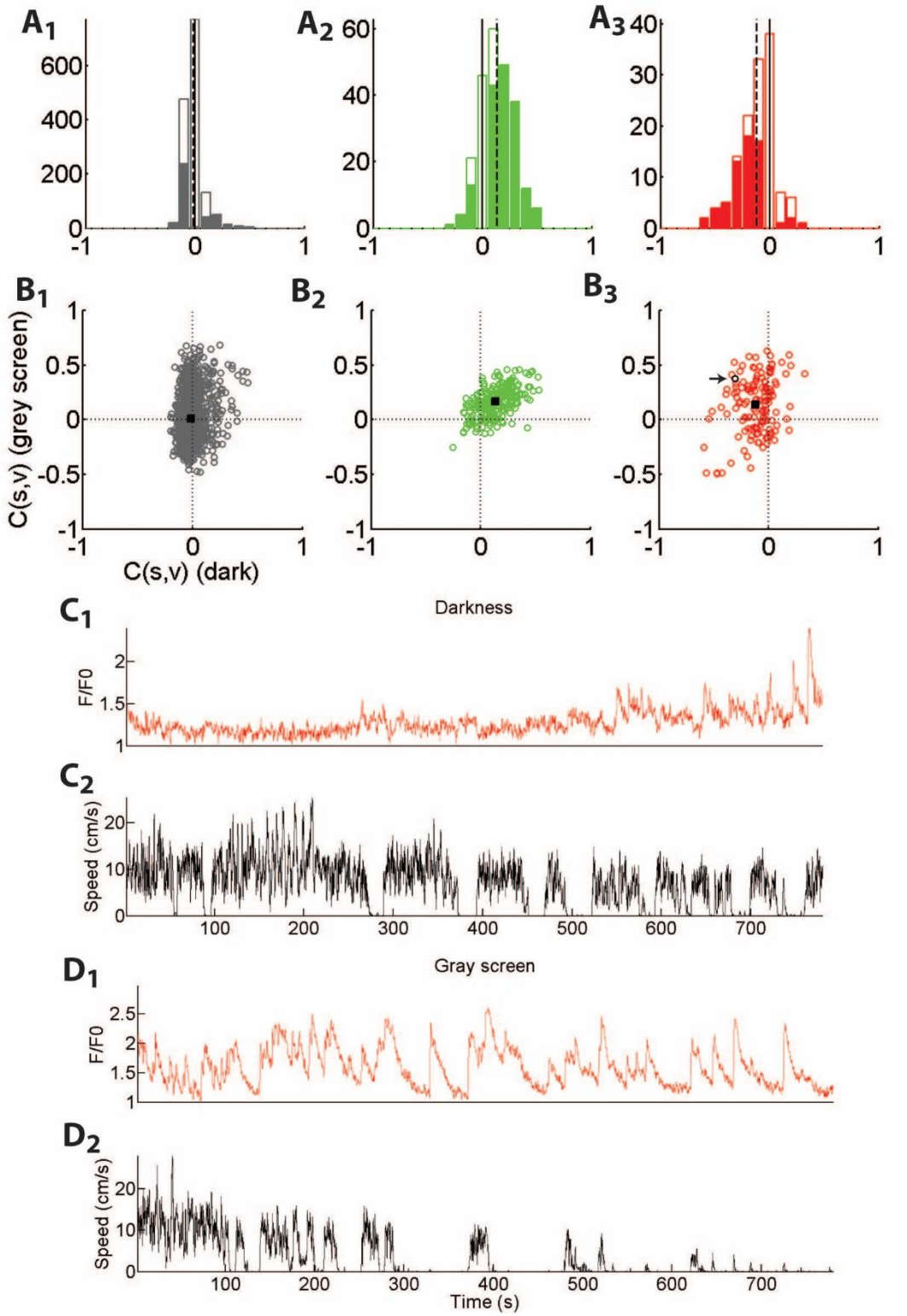

Supplementary Figure 3, related to Figure 2. Correlation of neural activity with running in darkness. (A) Histograms of correlations of neural activity with running speed in darkness. Filled portions of bars represent cells that are significantly modulated by speed ($p < 0.05$, shuffle test). (B) Correlation of neural activity with running during gray screen presentation vs. in darkness. Black squares represent population averages. Arrow in B_3 points to example *Sst* neuron whose traces are shown below. (C) Fluorescence trace (C_1) and running speed (C_2) for example *Sst* cell in darkness. (D) Fluorescence trace and running speed for the same cell when the screen was constantly gray.

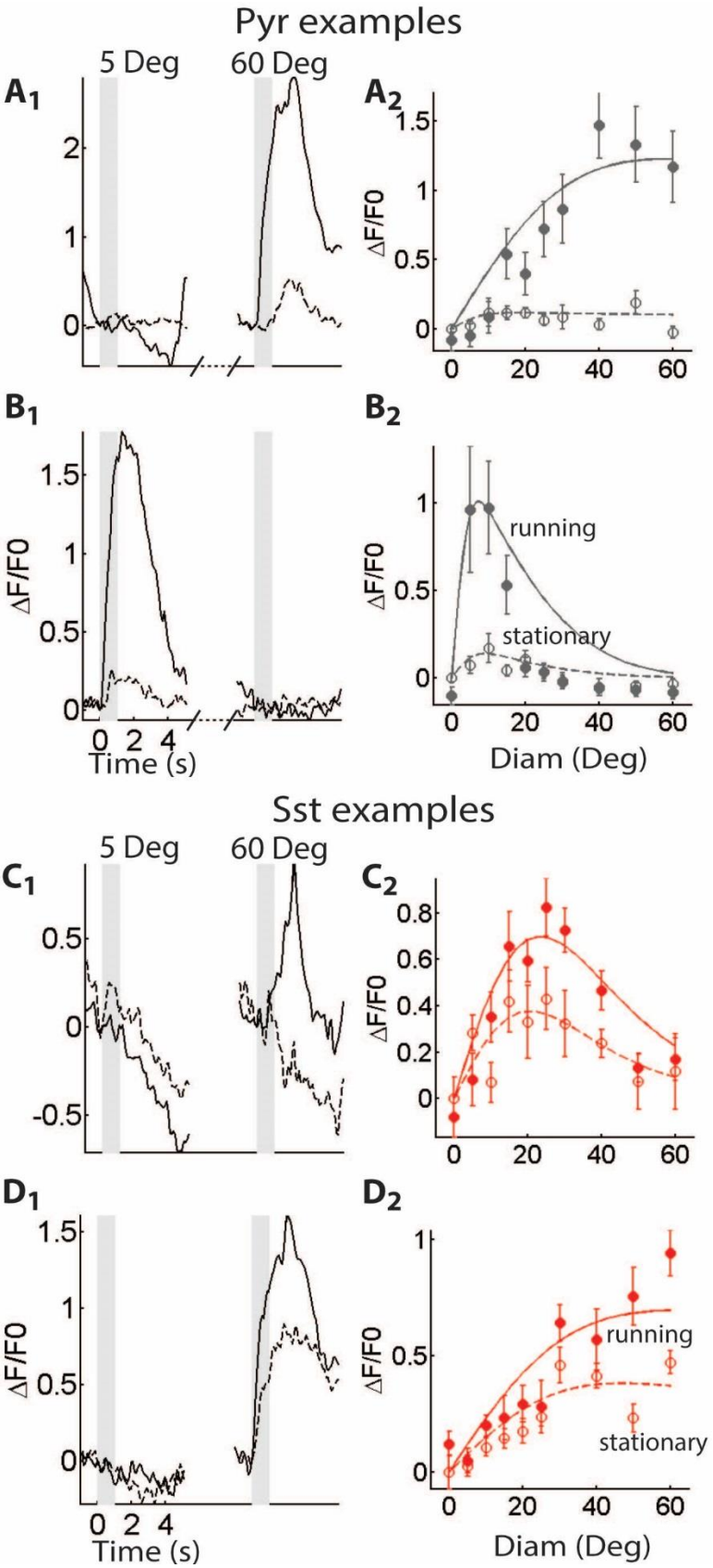

Supplementary Figure 4, related to Figure 3. Diversity of size tuning between cells. (A_1) Mean responses of a single Pyr neuron to 5° and 60° grating stimuli. Black curves show trial-averaged response in the stationary (dashed line) and running (continuous line) conditions. Grey shaded region of each subpanel indicates the 1 s stimulus presentation period. (A_2) size tuning curves for this example cell. Solid line: running; dashed line: stationary. (B) Same as (A) for another Pyr cell with different size tuning. (C,D) Same as (A) for two example *Sst* cells that showed diverse size tuning.

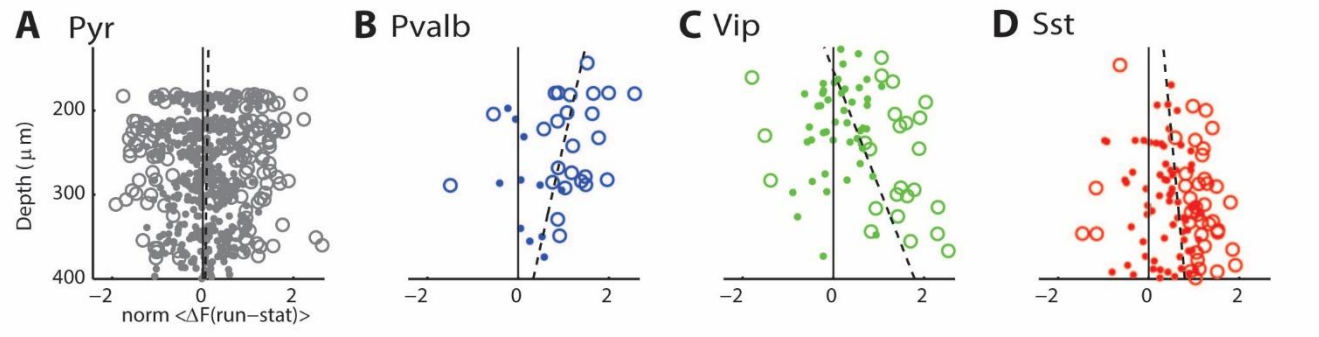

Supplementary Figure 5, related to Figure 3. Dependence of visual responses on cortical depth. In each panel, the x-axis shows the difference between average responses (across all stimuli) in running and stationary conditions, and the y-axis shows the cortical depth of each neuron. Circles represent neurons with a significant modulation of responses by running ($p < 0.05$, 1-way ANOVA). While we did not observe a significant effect of cortical depth on the modulation of sensory responses in Pyr ($p = 0.6$), and Sst ($p = 0.12$) cells, in Vip cells enhancement of responses by running significantly increased with cortical depth ($p < 10^{-4}$), while Pvalb cells showed a marginal decrease ($p = 0.07$).

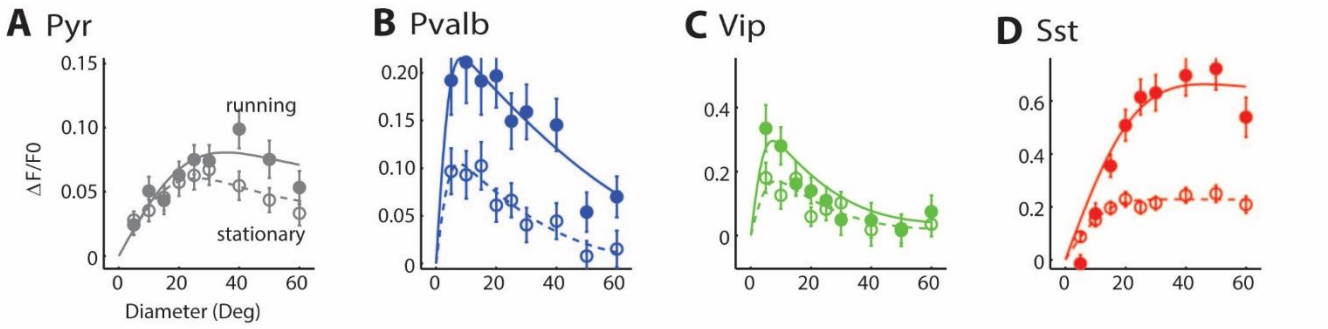

Supplementary Figure 6, related to Figure 3. Size tuning curves averaged over cells whose receptive fields were moderately off-center (distance from receptive field center to stimulus center between 10° and 20°). Solid line: running; dashed line: stationary.

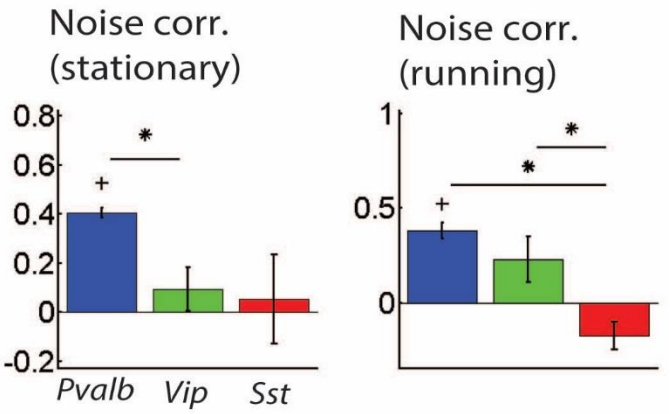

Supplementary Figure 7, related to Figure 4. Summary plots of noise correlations during stationary (left) and running (right) periods. Crosses represent populations whose correlations were significantly different from zero ($p < 0.05$, t-test), asterisks correspond to pairs of populations with significantly different correlations ($p < 0.05$, unpaired t-test).